Msi2 Maintains Quiescent State of Hair Follicle Stem Cells by Directly Repressing the Hh Signaling Pathway

Xianghui Ma[1,7], Yuhua Tian[1,7], Yongli Song[1], Jianyun Shi[1], Jiuzhi Xu[1], Kai Xiong[2], Jia Li[1], Wenjie Xu[1], Yiqiang Zhao[1], Jianwei Shuai[3], Lei Chen[4], Maksim V. Plikus[5], Christopher J. Lengner[6], Fazheng Ren[1], Lixiang Xue[2] and Zhengquan Yu[1]

Hair follicles (HFs) undergo precisely regulated cycles of active regeneration (anagen), involution (catagen), and relative quiescence (telogen). Hair follicle stem cells (HFSCs) play important roles in regenerative cycling. Elucidating mechanisms that govern HFSC behavior can help uncover the underlying principles of hair development, hair growth disorders, and skin cancers. RNA-binding proteins of the Musashi (Msi) have been implicated in the biology of different stem cell types, yet they have not been studied in HFSCs. Here we utilized gain- and loss-of-function mouse models to demonstrate that forced MSI2 expression retards anagen entry and consequently delays hair growth, whereas loss of *Msi2* enhances hair regrowth. Furthermore, our findings show that *Msi2* maintains quiescent state of HFSCs in the process of the telogen-to-anagen transition. At the molecular level, our unbiased transcriptome profiling shows that Msi2 represses Hedgehog signaling activity and that *Shh* is its direct target in the hair follicle. Taken together, our findings reveal the importance of *Msi2* in suppressing hair regeneration and maintaining HFSC quiescence. The previously unreported Msi2-Shh-Gli1 pathway adds to the growing understanding of the complex network governing cyclic hair growth.

Journal of Investigative Dermatology (2017) **137,** 1015–1024; doi:10.1016/j.jid.2017.01.012

INTRODUCTION

The hair follicle (HF) undergoes recurrent regenerative cycling consisting of anagen, catagen, and telogen phases (Stenn and Paus, 2001). Such cycling is sustained by the HF stem cells (HFSCs), which operate under complex signaling regulation. Many signaling pathways converge to jointly regulate HFSCs, including Wnt, Bmp, Notch, and Hedgehog (Hh) pathways among others (Lee and Tumbar, 2012; Millar, 2002; Plikus et al., 2008, 2017). Elucidating the in-depth mechanisms that govern HFSC behavior is essential for understanding the principles of normal hair development and etiology of human hair growth disorders. Morphologically, HFSCs are located in the so-called follicular bulge (BU), in close proximity to the mesenchymal dermal papilla—the principal signaling niche of the HF. Secondary hair germ (sHG) progenitors are located between HFSCs and dermal papilla, and during telogen, both HFSCs and sHG progenitors remain quiescent (Cotsarelis et al., 1990; Keyes et al., 2013). At the onset of anagen, signals from the dermal papilla, as well as the extrafollicular macroenvironment, activate proliferation of sHG cells, whose progenies expand downward, envelop dermal papilla, and generate a new hair matrix (Mx) (Plikus et al., 2011). To sustain anagen progression, sHG-derived transit-amplifying cells (TACs) in the Mx secrete Shh that acts to activate HFSCs in the BU (Hsu et al., 2014). Throughout anagen, TACs in the Mx proliferate move upward and terminally differentiate to form the inner root sheath and hair shaft. To a large degree, formation of TACs represents the bottleneck in the process of hair growth cycle, and without TAC-derived Shh, quiescent HFSCs fail to activate. However, little is known about the signals that counterbalance Shh to maintain HFSC quiescence.

Musashi (Msi) is an evolutionarily conserved RNA binding protein family, which was first identified in *Drosophila* (Nakamura et al., 1994). In mammals, there are two orthologs: MSI1/Msi1 (Sakakibara et al., 1996) and MSI2/Msi2

[1]*Beijing Advanced Innovation Center for Food Nutrition and Human Health and State Key Laboratories for Agrobiotechnology, College of Biological Sciences, China Agricultural University, Beijing, China;* [2]*Medical Research Center, Department of Radiation Oncology, Peking University Third Hospital, Beijing, China;* [3]*Department of Physics and State Key Laboratory of Cellular Stress Biology, Innovation Center for Cell Signaling Network, Xiamen University, Xiamen, China;* [4]*Department of Animal Science, Southwest University, Rongchang, Chongqing, China;* [5]*Department of Developmental and Cell Biology, Sue and Bill Gross Stem Cell Research, Center for Complex Biological Systems, University of California, Irvine, Irvine, California, USA; and* [6]*Department of Animal Biology, School of Veterinary Medicine, and Institute for Regenerative Medicine, University of Pennsylvania, Philadelphia, Philadelphia, USA*

[7]*These authors contributed equally to this work.*

Correspondence: Zhengquan Yu, College of Biological Sciences, China Agricultural University, No. 2 Yuanmingyuan West Road, Haidian District, Beijing 100193, China, E-mail: zyu@cau.edu.cn; Lixiang Xue, Department of Radiation Oncology, Peking University Third Hospital, No. 2 Huayuan North Road, Haidian District, Beijing 100191, China, E-mail: lixiangxue@bjmu.edu.cn; or Fazheng Ren, Beijing Advanced Innovation Center for Food Nutrition and Human Health, China Agricultural University, No.2 Yuanmingyuan West Road, Haidian District, Beijing 100193, China, E-mail: renfazheng@263.net

Abbreviations: BU, bulge; DTG, double transgenic; HF, hair follicle; HFSC, hair follicle stem cell; HG, secondary hair germ; Hh, Hedgehog; Msi, Musashi; Mx, hair matrix; Pn, postnatal day n; PWD, postwounding day; SC, stem cell; sHG, secondary hair germ; TAC, transit-amplifying cell; UTR, untranslated region

Received 24 May 2016; revised 27 December 2016; accepted 9 January 2017; accepted manuscript published online 29 January 2017; corrected proof published online 19 March 2017

(Sakakibara et al., 2001). Msi2 has been identified as the critical regulator of tissue-specific stem cells (SCs) in several systems, including neural system (Sakakibara et al., 2001), blood (Ito et al., 2010; Kharas et al., 2010; Park et al., 2014; Rentas et al., 2016), and intestine (Wang et al., 2015). Inactivation of MSI2 in hematopoietic stem cells impairs their competitive repopulation ability on transplantation (Hope et al., 2010; Ito et al., 2010; Kharas et al., 2010). Recently, MSI2 was shown to play important roles in several types of cancers (Kang et al., 2016; Katz et al., 2014; Kudinov et al., 2016; Wang et al., 2015). Although *Msi2* was shown to be expressed in HF BU, sHG, and inner root sheath (Sugiyama-Nakagiri et al., 2006), its role in HF development and regenerative cycling remains unknown. Here we demonstrate that *Msi2* is a key posttranscriptional regulator of HFSC quiescence and that it operates by directly targeting the Shh/Gli1 signaling pathway.

RESULTS

MSI2 overexpression retards the telogen-to-anagen transition during hair cycling

To elucidate the role of *Msi2* in hair cycling, we started by profiling its expression levels. *Msi2* is strongly expressed on postnatal day 21 (P21) during first telogen, reaches its highest levels at P36 during mid-anagen, and then decreases to its lowest levels at P42 and P49 (Figure 1a). At P21, Msi2 is primarily expressed in the BU and sHG (Figure 1b). At P36 and P40, it is prominently expressed both in the basal and suprabasal BU, outer root sheath, TACs, and inner root sheath (Figure 1b). At P49, when HFs enter the second telogen, Msi2 becomes localized to the basal and suprabasal BU and sHG—expression pattern that is reminiscent of that at P21. In addition, Msi2 is expressed in the basal epidermal cells at different time points (Supplementary Figure S1a and b online).

Next, we generated *K14-rtTA::TRE-MSI2* double transgenic (DTG) mice in which overexpression of the conserved human MSI2 can be induced throughout the epithelial compartment of the skin (Supplementary Figure S1c). On doxycycline induction, DTG mice exhibited robust *MSI2* overexpression in K14-positive skin, thymus, and esophagus, but not in K14-negative intestine (Supplementary Figure S1d). The induction of MSI2 in skin was further confirmed at protein level (Supplementary Figure S1e). Msi2 is specifically induced in the basal epidermal layer, outer root sheath, and follicular BU (Supplementary Figure S1f).

We induced MSI2 overexpression at P21 and characterized the resulting HF phenotype. At P24, control HFs displayed early anagen morphology, whereas DTG HFs were still in telogen (Figure 1c). At P26, both control and DTG HFs were in anagen, albeit DTG HFs were significantly shorter (Supplementary Figure S1g). When MSI2 overexpression was induced at P18, DTG phenotype became more pronounced with HFs displaying telogen morphology even at P26 (Figure 1d). Consistent with the delayed anagen entry, the length of DTG HFs was shorter than in control mice (Figure 1c and d). Supporting this phenotype, hair regrowth after shaving is delayed in the DTG animals (Supplementary Figure S1h). Together, these findings show that MSI2 overexpression significantly delays the telogen-to-anagen transition and progression through anagen.

MSI2 induction impairs hair regrowth after depilation

Next, we examined the role of Msi2 during the depilation-induced hair cycle. After depilation at P21, Msi2 becomes strongly expressed in sHG at P22 and in Mx at P24 (Supplementary Figure S2a online). We then induced MSI2 overexpression in DTG mice at P18 and depilated at P21. External hair regrowth was observed in littermate controls 10 days after depilation, but was still absent in DTG mice (Figure 2a). DTG mice eventually regrew hairs by P44 (Figure 2a). On histology, at P22 (i.e., 36 hours after depilation) both control and DTG HFs showed extended sHG, morphological feature of anagen II (Figure 2b and Supplementary Figure S2b). At P24, control HFs elongated and featured prominent hair bulb, a feature of anagen III. At the same time, DTG HFs lacked hair bulb (Figure 2b and Supplementary Figure S2b). Normally, anagen onset is accompanied by nuclear β-catenin, a marker of active Wnt signaling (Lo Celso et al., 2004; Lowry et al., 2005). Substantially fewer nuclear β-catenin positive cells can be found in DTG HFs at P24, whereas no differences are seen at P22 (Supplementary Figure S2c and d). Also, at P30, anagen DTG HFs are shorter than those in control mice (Figure 2b). Similar phenotype was observed when hairs were depilated during the second competent telogen phase (Supplementary Figure S2e and f). These findings indicate that overexpression of MSI2 delays anagen initiation.

Next we deleted *Msi2* in the skin of *K14-Cre::Msi2*$^{flox/flox}$ (cKO) mice (Supplementary Figure S3a online). Deletion specificity in skin was confirmed by quantitative real-time reverse transcriptase-PCR (Supplementary Figure S3b). Loss of Msi2 at the protein level was further confirmed by immunostaining and western blotting (Supplementary Figure S3c and d). Specific deletion of Msi2 was also found in the thymus, where K14 promoter is active (Supplementary Figure S3e), but not in the intestine (Supplementary Figure S3f). Although no obvious differences were found between control and cKO HFs during the natural hair cycle (Supplementary Figure S3g), the downward growth of *Msi2* cKO HFs is significantly faster than in control at 72 hours after depilation (Figure 2c and d). Also, the length of three types of hairs in cKO mice is significantly longer than in controls 21 days after depilation (Supplementary Figure S4a and b online). Similar phenotype was also found when hairs were depilated during the second competent telogen (Supplementary Figure S4c and d). Generally, cKO phenotype is opposite of that in DTG mice. We also noticed that anagen progression in control mice for cKO is slower than in control mice for DTG (Figure 2b and c, Supplementary Figure S4a). This is most likely due to background strain differences. DTG mice are on Friend leukemia virus B, whereas cKO mice are on mixed genetic background (C57BL/6xCBA, further crossed to Swiss Webster). For this reason, in all experiments we used littermate controls.

AE13 marks cuticle and cortex/precortex of the HF (Lynch et al., 1986), whereas AE15 marks inner root sheath and medulla cells (O'Guin et al., 1992), and both are used as sensitive markers of HF differentiation. At P24, AE13 and

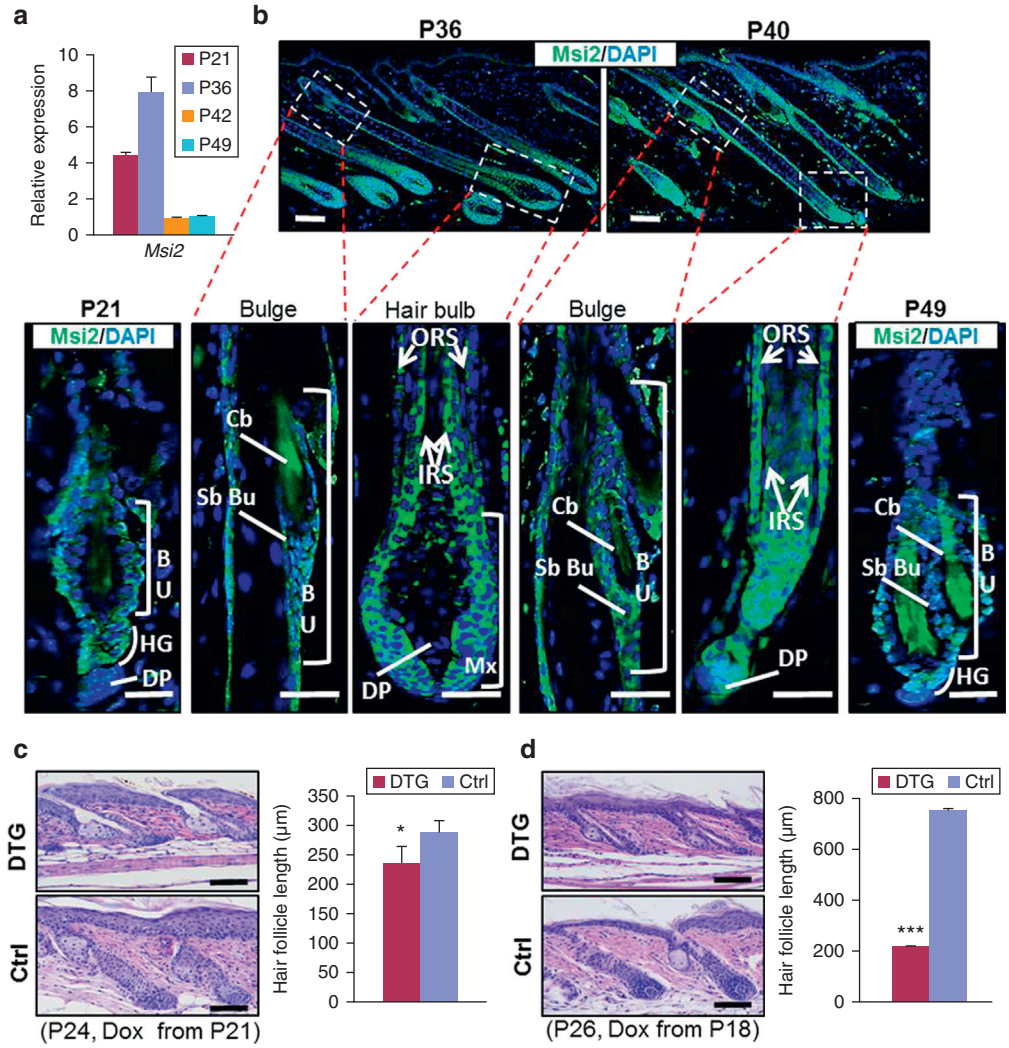

Figure 1. Forced MSI2 expression retards the telogen-to-anagen transition. (**a**) qRT-PCR for *Msi2* in WT mouse skin at indicated time points. (**b**) Immunostaining for Msi2 in WT HFs at indicated time points. The arrows point to Msi2 positive signals. The dashed boxes outline magnified regions. (**c, d**) Representative histologic images of dorsal skin from control (Ctrl) and DTG mice under indicated conditions. Quantification of HF length in gender-matched littermates between control (n = 3) and DTG mice (n = 3) at (**c**) P24 and (**d**) P26. n ≥ 3 biological replicates. $*P < 0.05$; $***P < 0.001$. Scale bars: 50 μm. BU, bulge; Dox, doxycycline; DP, dermal papilla; DTG, double transgenic mouse; HF, hair follicle; HG, hair germ; IRS, inner root sheath; Msi2, Musashi2; Mx, hair matrix; ORS, outer root sheath; Pn, postnatal day n; qRT-PCR, quantitative real-time reverse transcriptase-PCR; WT, wild type.

AE15 positive cells are present in control, but not in DTG HFs (Supplementary Figure S4e). In contrast, AE13-positive cells appear in *Msi2* cKO HFs ahead of littermate control (Supplementary Figure S4e). Consistently, DTG HFs display much fewer, whereas cKO HFs show more proliferative cells 3 days after depilation compared with littermate controls (Supplementary Figure S4f–h). Importantly, no differences in the number of proliferative cells were seen between DTG, cKO and corresponding control HFs on 90-minute BrdU pulse assay 24 hours after depilation (Figure 2e). Yet, substantially fewer and more BrdU-positive cells were seen in DTG and cKO HFs, respectively, after 48-hour pulse tracing (Figure 2f and g), suggesting impaired HFSC activation in response to Msi2 induction. Together, these data show that *MSI2* overexpression impairs, whereas loss of *Msi2* accelerates hair regrowth.

Msi2 maintains quiescent state of HFSCs

Previously, Msi2 has been an important regulator for neural, hematopoietic, and intestinal SCs. Here, we asked if it similarly regulates HFSCs. Intriguingly, we see that the number of α6-integrin^{+}CD34^{+} HFSCs is not significantly altered in both DTG and cKO mice as compared with control (Supplementary Figure S5a online). Next we asked if Msi2 regulates proliferative state rather than the number of HFSCs. K15 was used to identify rapidly cycling HFSCs (Greco et al., 2009; Liu et al., 2003). Sox9 was used as another marker for rapidly cycling HFSCs, with the expression pattern that is broader than of K15 (Vidal et al., 2005). In contrast, NFATc1 was used as the marker of quiescent HFSCs, located in the upper BU (Horsley et al., 2008). Three days after induction at P21, we observed more NFATc1-positive, yet fewer K15-positive HFSCs in DTG HFs (Supplementary Figure S5b). We also evaluated HFSCs in DTG and *Msi2* cKO mice 36 hours after depilation (P22), when no histologic differences were discernible. For DTG HFs, we also see more NFATc1-positive and fewer K15-positive HFSCs (Supplementary Figure S5c), and decreased HFSC proliferation (Figure 3a and b). In contrast, cKO HFs show fewer NFATc1-positive and more K15-positive HFSCs (Supplementary Figure S5d), and more proliferating HFSCs (Figure 3c and d). Together, these results indicate that *Msi2* functions to maintain HFSC quiescence. Previously, Lhx2 has been implicated as the regulator of HFCS quiescence (Folgueras et al., 2013; Mardaryev et al., 2011). Given functional similarity between Msi2 and Lhx2 activities, we examined whether the two are connected. We found fewer Lhx2-positive cells in DTG HFs 3

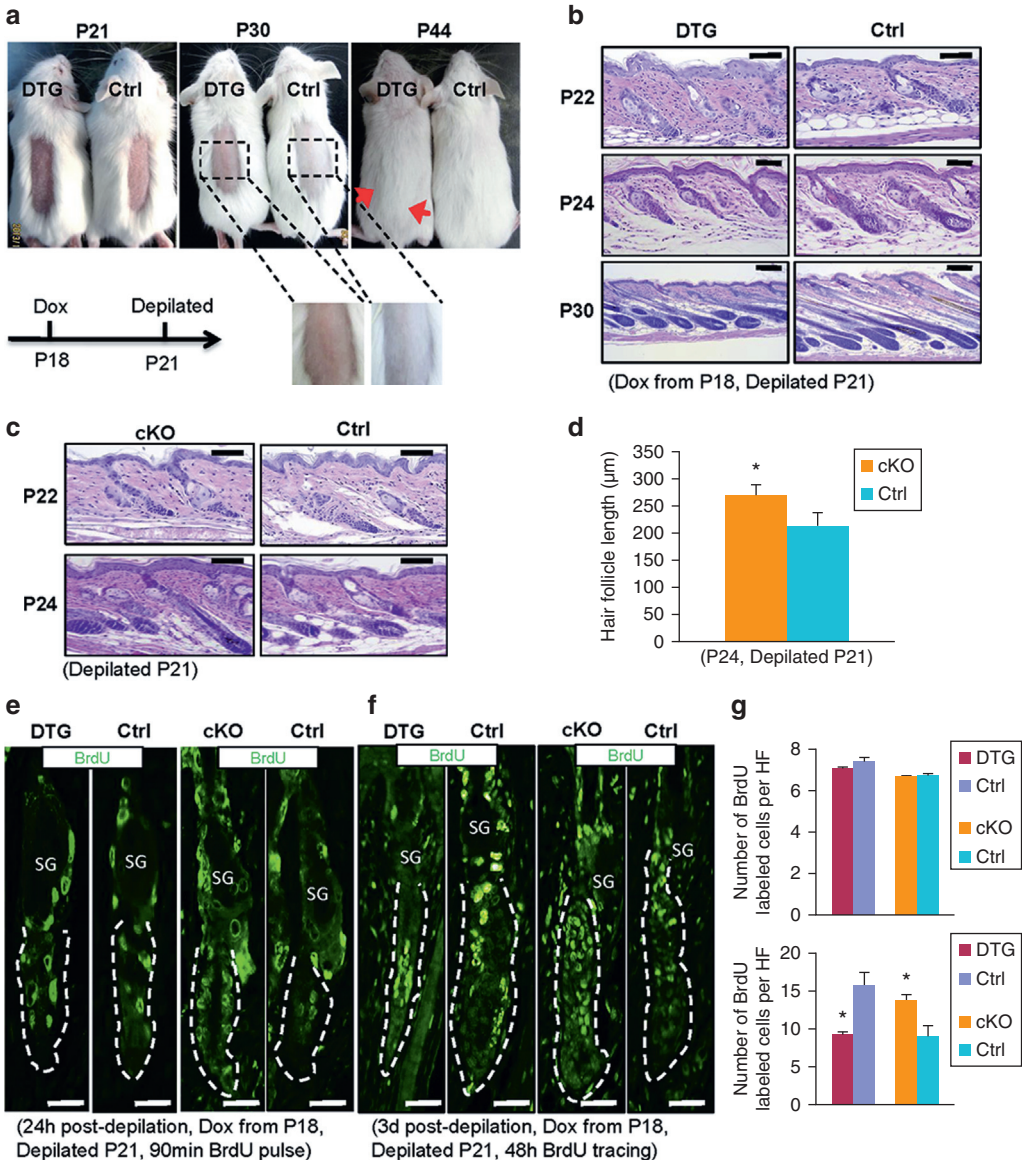

Figure 2. MSI2 induction impairs hair regrowth after depilation. (**a**) Gross images of depilated Dox-treated (from P18) control (n = 5) and DTG mice (n = 4) at indicated time points. The red arrows mark depilation boundaries. (**b, c**) Histology of dorsal skin from (**b**) control and DTG, and (**c**) control and cKO mice at indicated time points after depilation. (**d**) Statistics of HF length in control (n = 3) and cKO mice (n = 3) at P24. (**e, f**) Immunofluorescence for BrdU in control and DTG, or control and cKO HFs at indicated conditions after (**e**) 90 minutes and (**f**) 48 hours of BrdU pulse. The dashed lines mark HFs. n = 3. (**g**) Quantification of BrdU labeled cells per HF (BU+sHGs) for (**e,** top) and (**f,** bottom). *$P < 0.05$. Scale bars: 50 μm. BU, bulge; Dox, doxycycline; DTG, double transgenic mouse; HF, hair follicle; MSI2, Musashi2; Pn, postnatal day n; sHG, secondary hair germ.

days after doxycycline induction at P21 (Supplementary Figure S6a online) or 36 hours after depilation (Supplementary Figure S6b), and more Lhx2-positive cells in cKO HFs 36 hours after depilation (Supplementary Figure S6c), suggesting that Msi2 does not regulate Lhx2, and that the two likely maintain HFCS quiescence via distinct mechanisms.

Msi2 represses HF neogenesis

Next, we asked whether MSI2 induction inhibits wound-induced HF neogenesis, the regenerative phenomenon that resembles embryonic HF development (Horsley et al., 2008). We induced *MSI2* overexpression at P18 and wounded mice at P21. Scab detachment in DTG mice was 2 days delayed as compared with controls (Supplementary Figure S7a online). At postwounding day (PWD) 17, HF neogenesis was largely abrogated in DTG mice (Supplementary Figure S7b). Although the number of de novo HFs in DTG mice is much fewer than in control wounded mice at PWD 17, we noticed that more de novo HFs regenerated in DTG wounds by PWD 33 (Supplementary Figure S7c). To further differentiate if HF neogenesis is suppressed by MSI2 rather than simply delayed, we induced MSI2 overexpression 10 days after wounding, just days ahead of HF neogenesis onset. With this induction timing, initial wound closer was not affected in DTG mice (Supplementary Figure S7d). Yet, there were still significantly fewer de novo HFs forming in DTG mice, supporting the notion that MSI2 overexpression indeed represses HF neogenesis (Supplementary Figure S7d). In contrast, more de novo HFs were seen to form in the wounds of *Msi2* cKO mice as compared with littermate controls at PWD 15 (Supplementary Figure S7e), despite the same wound closure rates. This trend also continued at PWD 17 (Supplementary Figure S7f). Taken together, these findings demonstrate that Msi2 represses wound-induced HF neogenesis.

MSI2 induction represses the Shh/Gli1 signaling pathway

To gain mechanistic insights into the molecular events underlying repression of the telogen-to-anagen transition by

Msi2, we performed transcriptome profiling on control and DTG dorsal skin 3 days after doxycycline treatment (P21–P24). It reveals that *Msi2* induction drives rapid and robust changes in gene expression (Supplementary Figure S8a and b online). We identified 209 downregulated and 319 upregulated genes with a significance $P < 0.05$ and a fold change >2.0 (Supplementary Figure S8a). Gene ontology analysis on these 528 genes identified "keratinization" and "skin development" among the top affected biological processes (Supplementary Figure S8c). Surprisingly, many of the signaling pathways, including Notch, mTOR, and transforming growth factor-β, which had been implicated as targets of Msi2 in other organs (Okano et al., 2005; Park et al., 2014; Wang et al., 2015), are not affected by MSI2 overexpression in skin (Supplementary Figure S8d). This result was further confirmed by quantitative real-time reverse transcriptase-PCR and western blotting (Supplementary Figure S8e and f), and it indicates a tissue-specific mechanism for Msi2 function in the skin.

Enrichment for "basal cell carcinoma" and "Hh signaling pathway" on gene ontology analysis (Supplementary Figure S8d), the known role of dysregulated Hh signaling in basal cell carcinoma (Epstein, 2008), and the established role of Hh signaling in HFSC activation (Hsu et al., 2014) all point toward a potential link between Msi2 and Hh signaling pathway in HFs. Many downstream Hh target genes *Shh*, *Gli1*, *Ptch2*, and *Hhip* are downregulated in DTG skin (Figure 4a). In contrast, several downstream Hh targets *Shh*, *Gli1,* and *Ptch2* are upregulated in *Msi2* cKO skin (Figure 4b). Together, these data suggest that Msi2 inhibits Hh signaling.

Interestingly, the upstream gene *Shh* was downregulated in DTG mice, whereas it was upregulated in *Msi2* cKO mice both on RNA and protein levels (Figure 4a–d). Considering that Msi2 functions as a negative regulator of gene expression via repression of protein translation (Ito et al., 2010; Kharas et al., 2010; Wang et al., 2015) or mRNA destabilization (Bennett et al., 2016) by directly binding to 3′-untranslated region (UTR) of target genes (Ito et al., 2010; Kharas et al., 2010; Okano et al., 2005; Wang et al., 2015), we proposed that *Shh* might be a direct target of Msi2. The binding motif of Msi2 has been identified as 5′-(G/A)U_nAGU-3′ (n = 1–3) (Imai et al., 2001; Sakakibara et al., 2001). After screening for Msi2 binding sites, we identified a perfectly matched motif of (5′-GUUUAGT-3′) in the conserved region of *Shh* 3′-UTR (Figure 4e). Homology analysis demonstrated that the identified motif is conserved among placental mammals (Supplementary Figure S9a and b online). To further test whether 3′-UTR of *Shh* is a direct target of Msi2, we constructed luciferase reporters for the *Shh* 3′-UTRs, as well as reporter constructs in which the Msi2 binding sites were mutated. We found that wild-type *Shh* 3′-UTR reporter activity was significantly repressed, but no significant change for the mutant-type reporters was seen with overexpression of hMSI2 (Figure 4e). This indicates that Msi2 might directly target *Shh*. Furthermore, RNA crosslinking immunoprecipitation (CLIP)-PCR assay revealed that *Shh* is enriched in the Msi2 antibody immunoprecipitates (Figure 4f), demonstrating that Msi2 physically binds to 3′-UTR of *Shh* mRNA. Thbs1, a known Msi2 target in skin, was used as the positive control (Bennett et al., 2016). Interestingly, *Numb* and *Pten*, which have been identified as Msi2 targets in intestine (Wang et al., 2015), were not enriched in the Msi2 antibody immunoprecipitates of skin keratinocytes (Figure 4f). These data suggest that Msi2 has unique targets in different organs. In situ hybridization further revealed that Msi2 and *Shh* colocalize in the Mx and activated sHG of HFs (Figure 4g, Supplementary Figure S10a and b online), implying direct interaction between Msi2 and *Shh* in the process of HF development. Furthermore, we reveal that Msi2 induction promotes decays of *Shh* mRNA (Figure 4h). Consistently, *Shh* mRNA is reduced in DTG HFs at 36 hours and 3 days after depilation, and upregulated in Msi2 cKO HFs (Supplementary Figure S10a and b). Together, these findings demonstrate that Msi2 represses gene expression of Shh by destabilizing *Shh* mRNA.

Next, we asked whether *Shh* repression mediated by Msi2 functionally regulates hair regrowth after depilation. *Shh* is induced starting 24 hours after depilation when sHG enlarges and TACs form (Hsu et al., 2014). Thus, we examined expression of *Shh* in DTG and cKO HFs 36 hours after depilation. We observe a prominent reduction of *Shh* in DTG mice and a moderate increase in cKO mice at the mRNA and protein levels (Figure 5a–c). Gli1 is a readout target of Shh signaling. We found that Gli1 is highly expressed in the TACs of Mx in control, but not DTG HFs (Figure 5a and c, Supplementary Figure S10c). In contrast, Gli1 is increased in the Mx of cKO HFs (Figure 5b and c, Supplementary Figure S10c). Cyclin D1 is another known downstream target of Shh (Hsu et al., 2014; Kenney and Rowitch, 2000). In agreement, Cyclin D1 is reduced in sHG of DTG and increased in sHG of cKO regenerated HFs (Figure 5c and d). Shh signaling also downregulates bone morphogenic protein-specific p-Smad1/5/8, which is required for early anagen progression (Kenney and Rowitch, 2000). Consistently, p-Smad1/5/8 is upregulated in DTG and downregulated in cKO HFs (Figure 5c and e). Considering that Msi1 is another mammalian ortholog of Msi2 and it functions redundantly in some tissues (Sakakibara et al., 2001; Wang et al., 2015), we tested Msi1 expression. We show that it is not altered in both DTG and cKO mice (Figure 5c). To further confirm this model, we performed a rescue experiment with Hh agonist, smoothened agonist (Heine et al., 2011; Paladini et al., 2005). Western blotting for Gli1 confirmed that smoothened agonist activated Hh signaling (Supplementary Figure S10d). In comparison with control mice, vehicle-treated dorsal skin of DTG mice exhibited delayed external hair regrowth and delayed anagen progression (Figure 5f). However, smoothened agonist-treated dorsal skin showed faster hair regrowth in DTG mice (Figure 5f). These findings suggest that activation of the Hh signaling pathway is able to rescue hair cycle inhibition caused by MSI2 overexpression (Figure 5f). Together, our findings show that Msi2 represses Hh pathway activity to regulate hair regrowth after depilation.

In summary, our findings reveal the importance of Msi2 in suppressing hair regeneration and maintaining HFSC quiescence during the telogen-to-anagen transition. We provide in vivo evidence for a previously unreported mechanism of

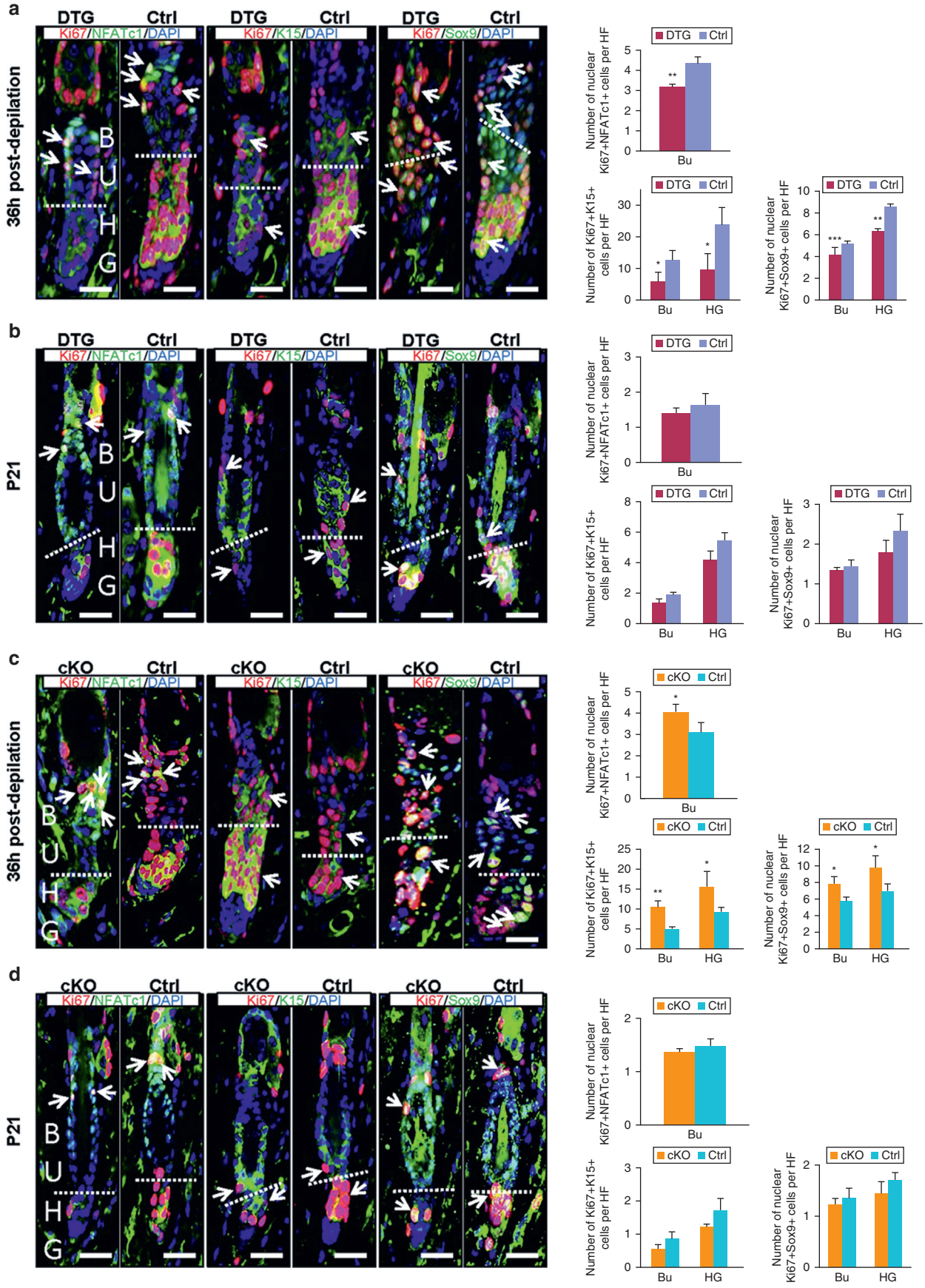

Figure 3. Msi2 maintains quiescent state of HFSCs. (**a, b**) Coimmunofluorescence for NFATc1/Ki67, K15/Ki67, and Sox9/Ki67 in control and DTG HF under conditions of 36 hours (**a**) after depilation at P21 and (**b**) before depilation at P21, pretreated with Dox at P18. (**c, d**) Coimmunofluorescence for NFATc1/Ki67,

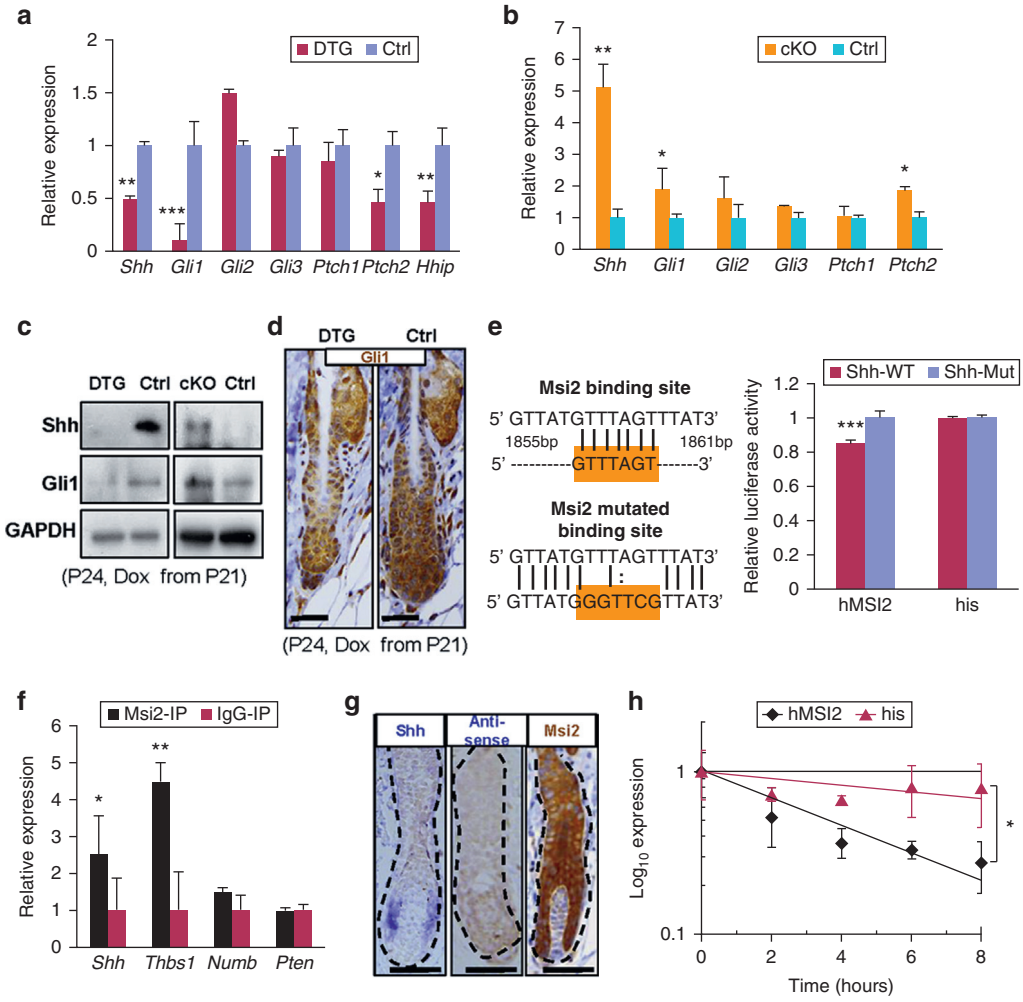

Figure 4. Msi2 directly targets Shh. (**a, b**) qRT-PCR for *Shh* and the Hh downstream genes in (**a**) DTG mice after Dox treatment (P21–P24) and (**b**) cKO mice at P24. (**c**) Western blotting for Shh and Gli1 in DTG and cKO skin at P24. (**d**) Immunostaining for Gli1 in DTG follicles at P24. Scale bar: 50 μm. (**e**) The WT and mutant binding sites of *Msi2* in 3′-UTR of *Shh*. Luciferase reporter activity of *Msi2* WT and mutant 3′-UTR constructs. His: vector without *MSI2*. (**f**) CLIP-PCR assay for Shh, Thbs1, Numb upon Msi2 antibody immunoprecipitates. (**g**) In situ hybridization for Shh and IHC for Msi2 in WT HFs at P24. (**h**) Shh RNA decay curve on human MSI2 overexpression treatment. n = 3. $*P < 0.05$, $**P < 0.01$, $***P < 0.001$. Dox, doxycycline; DTG, double transgenic mouse; GAPDH, glyceraldehyde-3-phosphate dehydrogenase; HF, hair follicle; Hh, Hedgehog; IHC, immunohistochemistry; Msi2, Musashi2; Pn, postnatal day n; qRT-PCR, quantitative real-time reverse transcriptase-PCR; UTR, untranslated region; WT, wild type.

Shh-Gli1 pathway repression by Msi2 (Figure 5g), adding to the growing understanding of the complex signaling network that governs cyclic hair growth.

DISCUSSION

Transient activation of quiescent HFSCs is necessary for sustained cyclic activation of HF regrowth (Rompolas and Greco, 2014). The signaling network that drives their activation consists of multiple pathways, including but not limited to Shh and Wnt (Rompolas and Greco, 2014). Particularly, Shh has recently been identified as an important signal that emanates from TACs during early anagen and drives proliferative activation of the adjacent BU HFSCs (Hsu et al., 2014). Here we found that *Msi2* maintains quiescent state of HFSCs by directly targeting Shh. Interestingly, Msi2 expression levels are elevated during physiological anagen and in response to hair cycle activation by depilation states when HFSCs undergo activation. Thus, our findings suggest that rather than locking HFSCs in prolonged quiescence during telogen, Msi2 fine-tunes HFSC activation by Shh during anagen initiation.

Previous studies implicated Msi2 as a critical regulator of murine hematopoietic and intestinal stem cell self-renewal and fate determination (Ito et al., 2010; Kharas et al., 2010; Park et al., 2014; Wang et al., 2015). Msi2 is a general regulator of somatic SCs in a variety of organs. Importantly, in contrast to its role in promoting SC quiescence in the HF, Msi2 promotes proliferation of hematopoietic stem cells and intestinal stem cells in the bone marrow and intestine, respectively (Ito et al., 2010; Kharas et al., 2010; Park et al., 2014; Wang et al., 2015). This indicates that specific Msi2 functions in tisse SC type-dependent. Opposing roles for Msi2 were shown in the context of cancer. Msi2 has been identified as a tumor suppressor in breast cancer, where it represses the epithelial-to-mesenchymal transition (Katz et al., 2014). However, in colorectal cancer and leukemia, it functions as an oncoprotein (Ito et al., 2010; Kharas et al., 2010; Park et al., 2014; Wang et al., 2015).

K15/Ki67, and Sox9/Ki67 in control and cKO HFs 36 hours (**c**) after depilation at P21and (**d**) before depilation at P21. The dashed line denotes the boundary of BU and HG. The arrows mark the double positive signal. (**a**–**d**) Quantification of NFATc1$^+$Ki67$^+$, K15$^+$/Ki67$^+$, and Sox9$^+$Ki67$^+$ cells in the corresponding conditions. n = 3. $*P < 0.05$; $**P < 0.01$; $***P < 0.001$. Scale bar: 50 μm. BU, bulge; Dox, doxycycline; DTG, double transgenic mouse; HF, hair follicle; HG, hair germ; HFSC, hair follicle stem cell; Msi2, Musashi2; Pn, postnatal day n.

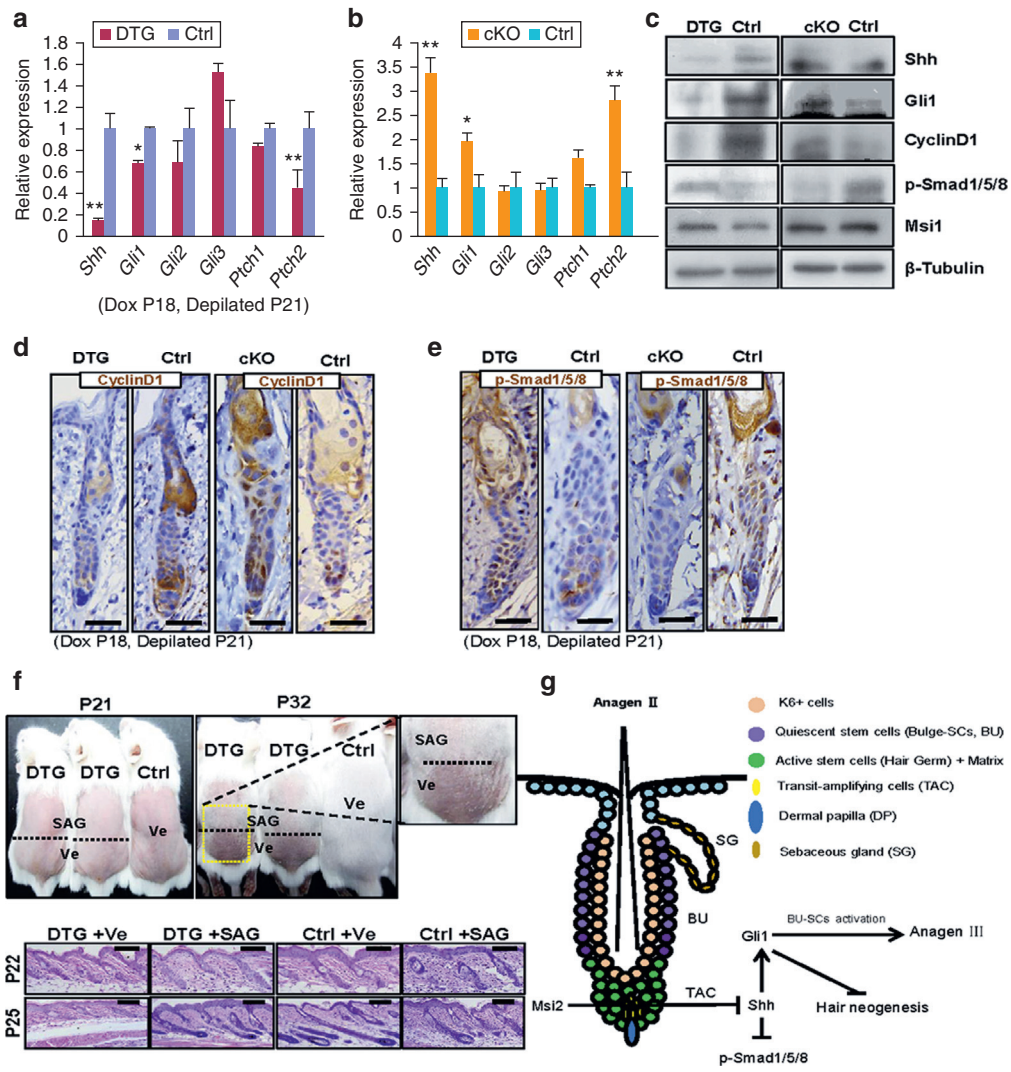

Figure 5. Msi2 represses Hh signaling after depilation. (**a, b**) qRT-PCR for *Shh* and Hh downstream genes in (**a**) DTG mice and (**b**) cKO mice 36 hours after depilation at P21. (**c**) Western blotting for Shh, Gli1, Cyclin D1, p-Smad1/5/8, and Msi1, and IHC for (**d**) Cyclin D1 and (**e**) p-Smad1/5/8 in DTG and cKO skin 36 hours after depilation at P21. (**f**) Administration of SAG rescues the delayed hair regrowth after depilation at P21. The dashed line denotes boundary of SAG (Upper) and Ve (Lower) treatment. Histology of skin from control and DTG mice under indicated conditions at P22 (36 hours after depilation) and P25 (DTG, n = 4; control, n = 7). Scale bar: 50 μm. (**g**) Schematic of the *Msi2* working model in HFSCs. n = 3. $^{*}P < 0.05$, $^{**}P < 0.01$. BU, bulge; DTG, double transgenic mouse; IHC, immunohistochemistry; Hh, Hedgehog; HFSC, hair follicle stem cell; Msi2, Musashi2; Pn, postnatal day n; qRT-PCR, quantitative real-time reverse transcriptase-PCR; SAG, smoothened agonist; SG, sebaceous gland; TAC, transit-amplifying cell; Ve, vehicle.

Mechanistically, we show that Msi2 promotes HFSC quiescence by directly repressing *Shh*. MSI2 overexpressing HFs display reduced proliferation in the BU and hair bulb, resembling phenotype of Shh-cKO mice (Hsu et al., 2014). In contrast, increased HFSC proliferation is seen in *Msi2* cKO HFs after depilation. TAC pool would wane if they cannot produce Shh, which could explain the delayed growth of HFs in MSI2 overexpressing mice after depilation. On the basis of our data, we propose a model where restriction of Shh signaling by Msi2 fine-tunes the process of quiescent HFSC activation (Figure 5g). We noticed that the Hh downstream target Ptch1 is not significantly altered in both DTG and cKO mice. This suggests that the regulation of Hh downstream targets is complex, and likely context dependent. Overactive Hh signaling is essential for basal cell carcinoma development (Epstein, 2008; Kasper et al., 2012), and overexpression of Shh, Gli1, and/or Smo induced basal cell carcinomas in mice (Dahmane et al., 1997; Oro et al., 1997). We speculate that Msi2 can act as the potential inhibitor of basal cell carcinomas—a possibility that can be examined in the future studies.

Previous works identified several targets for Msi2, including Numb, Pten, and transforming growth factor-β. *Msi2* repress translation of *Numb* in neural precursors (Okano et al., 2005) and in malignant hematopoietic cells (Ito et al., 2010; Kharas et al., 2010). Msi2 governs hematopoietic stem cell self-renewal and cell fate determination by modulating cells' sensitivity to transforming growth factor-β signaling (Park et al., 2014). It also drives intestinal transformation by targeting tumor suppressor, *Pten* (Wang et al., 2015). However, the above targets are not altered in the skin of MSI2 overexpressing mice and *Msi2* cKO mice, further highlighting tissue specificity of the Msi2 mechanism of action. In summary, we reveal that Msi2 plays an important role in maintaining quiescent state of HFSCs via the Msi2-Shh-Gli1 signaling axis during HF regeneration.

MATERIALS AND METHODS

Details regarding materials and methods are provided in the Supplementary Materials and Methods online.

All animal procedures were evaluated and authorized by the Beijing Laboratory Animal Management. All animal studies were performed in strict adherence to the Institutional Animal Care and

Use Committee guidelines of China Agricultural University (approval number: SKLAB-2011-04-03).

Wounding and whole-mount HF neogenesis assay

Wound-induced hair neogenesis assay was performed as previously described (Horsley et al., 2008; Yuan et al., 2015). Full-thickness 2.25 cm^2 wounds were created on dorsal skin at P21 in mice anaesthetized with sodium pentobarbital. For de novo HF analysis, mice were killed at 15 or 17 days after wounding.

Dual luciferase activity assay

Shh 3′-UTR fragment containing the binding site 5′-GUUUAGT-3′ was cloned into the psiCHECK-2 vector (Promega, Madison, WI). The mutant binding site was 5′-GGGTTCG-3′, obtained by a Quik-Change Site-Directed Mutagenesis kit (Stratagene, St Clara, CA). Ten nanograms of *Shh* and mutant reporter constructs were cotransfected with human MSI2 overexpressing vector (hMSI2) or a negative control (his) into 293T cells, respectively. The activity of Firefly and Renilla luciferase was measured with the Dual-Glo luciferase assay system (Promega). The primers were: forward: 5′- AAAGCGCACG GAAGGAG-3′; reverse: 5′-CGCAGGACAAGGGACAT-3′.

CLIP-qPCR

CLIP-qPCR assay was performed as previously described with modification (Wang et al., 2015). Briefly, cell suspensions of lower HF were irradiated twice at 400 mJ/cm^2, and then lysed using PXL buffer. After spinning, the supernatant was added to protein A Dynabeads (Dynal, 100.02, Thermo Fisher, Fremont, CA), conjugated with an anti-Msi2 antibody (Abcam, Cambridge, UK) or goat antirabbit IgG (Jackson ImmunoResearch, West Grove, PA) and incubated for 4 hours at 4 °C. Beads were washed and digested with Proteinase K. RNA was extracted from beads and then quantified with quantitative real-time reverse transcriptase-PCR.

RNA stability measurements

The RNA decay curve assay was performed as previously described (Bennett et al., 2016). Briefly, Lovo cells were transfected with 1 μg human MSI2 overexpressing vector (hMSI2) or a negative control (his). RNA was measured at 0, 2, 4, 6, and 8 hours using quantitative real-time reverse transcriptase-PCR.

CONFLICT OF INTEREST

The authors state no conflict of interest.

ACKNOWLEDGMENTS

ZY is supported by the Major Project for Cultivation Technology (2016ZX08008001 , 2014ZX08008001); NSFC (Nos. 81572614, 31271584); Beijing Nature Foundation Grant (5162018); Basic Research Program (2015QC0104, 2015TC041, 2016SY001, 2016QC086); SKLB Open Grant (2015SKLB6-16). LX is supported by the NSFC (No. 81541142, 81672091). MVP is supported by the NIH NIAMS grants R01-AR067273 and R01-AR069653. We thank Shukai Yuan, Feifei Li, and Liang Zhong for their kind help in sharing methods and in submitting the RNA-Seq data and Liying Du in the Core Facilities at School of Life Sciences, Peking University, for sorting the hair follicle stem cells.

SUPPLEMENTARY MATERIAL

Supplementary material is linked to the online version of the paper at www.jidonline.org, and at http://dx.doi.org/10.1016/j.jid.2017.01.012.

REFERENCES

Bennett CG, Riemondy K, Chapnick DA, Bunker E, Liu X, Kuersten S, et al. Genome-wide analysis of Musashi-2 targets reveals novel functions in governing epithelial cell migration. Nucleic Acids Res 2016;44:3788–800.

Cotsarelis G, Sun TT, Lavker RM. Label-retaining cells reside in the bulge area of pilosebaceous unit: implications for follicular stem cells, hair cycle, and skin carcinogenesis. Cell 1990;61:1329–37.

Dahmane N, Lee J, Robins P, Heller P, Ruiz i Altaba A. Activation of the transcription factor Gli1 and the Sonic hedgehog signalling pathway in skin tumours. Nature 1997;389:876–81.

Epstein EH. Basal cell carcinomas: attack of the hedgehog. Nat Rev Cancer 2008;8:743–54.

Folgueras AR, Guo X, Pasolli HA, Stokes N, Polak L, Zheng D, et al. Architectural niche organization by LHX2 is linked to hair follicle stem cell function. Cell Stem Cell 2013;13:314–27.

Greco V, Chen T, Rendl M, Schober M, Pasolli HA, Stokes N, et al. A two-step mechanism for stem cell activation during hair regeneration. Cell Stem Cell 2009;4:155–69.

Heine VM, Griveau A, Chapin C, Ballard PL, Chen JK, Rowitch DH. A small-molecule smoothened agonist prevents glucocorticoid-induced neonatal cerebellar injury. Sci Transl Med 2011;3:105ra4.

Hope KJ, Cellot S, Ting SB, MacRae T, Mayotte N, Iscove NN, et al. An RNAi screen identifies Msi2 and Prox1 as having opposite roles in the regulation of hematopoietic stem cell activity. Cell Stem Cell 2010;7:101–13.

Horsley V, Aliprantis AO, Polak L, Glimcher LH, Fuchs E. NFATc1 balances quiescence and proliferation of skin stem cells. Cell 2008;132:299–310.

Hsu YC, Li L, Fuchs E. Transit-amplifying cells orchestrate stem cell activity and tissue regeneration. Cell 2014;157:935–49.

Imai T, Tokunaga A, Yoshida T, Hashimoto M, Mikoshiba K, Weinmaster G, et al. The neural RNA-binding protein Musashi1 translationally regulates mammalian numb gene expression by interacting with its mRNA. Mol Cell Biol 2001;21:3888–900.

Ito T, Kwon HY, Zimdahl B, Congdon KL, Blum J, Lento WE, et al. Regulation of myeloid leukaemia by the cell-fate determinant Musashi. Nature 2010;466:765–8.

Kang MH, Jeong KJ, Kim WY, Lee HJ, Gong G, Suh N, et al. Musashi RNA-binding protein 2 regulates estrogen receptor 1 function in breast cancer [e-pub ahead of print]. Oncogene; http://dx.doi.org/10.1038/onc.2016.327 (accessed 5 September 2016).

Kasper M, Jaks V, Hohl D, Toftgard R. Basal cell carcinoma—molecular biology and potential new therapies. J Clin Invest 2012;122:455–63.

Katz Y, Li F, Lambert NJ, Sokol ES, Tam WL, Cheng AW, et al. Musashi proteins are post-transcriptional regulators of the epithelial-luminal cell state. Elife 2014;3:e03915.

Kenney AM, Rowitch DH. Sonic hedgehog promotes G(1) cyclin expression and sustained cell cycle progression in mammalian neuronal precursors. Mol Cell Biol 2000;20:9055–67.

Keyes BE, Segal JP, Heller E, Lien WH, Chang CY, Guo X, et al. Nfatc1 orchestrates aging in hair follicle stem cells. Proc Natl Acad Sci USA 2013;110:E4950–9.

Kharas MG, Lengner CJ, Al-Shahrour F, Bullinger L, Ball B, Zaidi S, et al. Musashi-2 regulates normal hematopoiesis and promotes aggressive myeloid leukemia. Nat Med 2010;16:903–8.

Kudinov AE, Deneka A, Nikonova AS, Beck TN, Ahn YH, Liu X, et al. Musashi-2 (MSI2) supports TGF-beta signaling and inhibits claudins to promote non-small cell lung cancer (NSCLC) metastasis. Proc Natl Acad Sci USA 2016;113:6955–60.

Lee J, Tumbar T. Hairy tale of signaling in hair follicle development and cycling. Semin Cell Dev Biol 2012;23:906–16.

Liu Y, Lyle S, Yang Z, Cotsarelis G. Keratin 15 promoter targets putative epithelial stem cells in the hair follicle bulge. J Invest Dermatol 2003;121:963–8.

Lo Celso C, Prowse DM, Watt FM. Transient activation of beta-catenin signalling in adult mouse epidermis is sufficient to induce new hair follicles but continuous activation is required to maintain hair follicle tumours. Development 2004;131:1787–99.

Lowry WE, Blanpain C, Nowak JA, Guasch G, Lewis L, Fuchs E. Defining the impact of beta-catenin/Tcf transactivation on epithelial stem cells. Genes Dev 2005;19:1596–611.

Lynch MH, O'Guin WM, Hardy C, Mak L, Sun TT. Acidic and basic hair/nail ("hard") keratins: their colocalization in upper cortical and cuticle cells of the human hair follicle and their relationship to "soft" keratins. J Cell Biol 1986;103:2593–606.

Mardaryev AN, Meier N, Poterlowicz K, Sharov AA, Sharova TY, Ahmed MI, et al. Lhx2 differentially regulates Sox9, Tcf4 and Lgr5 in hair follicle stem cells to promote epidermal regeneration after injury. Development 2011;138:4843–52.

Millar SE. Molecular mechanisms regulating hair follicle development. J Invest Dermatol 2002;118:216–25.

Nakamura M, Okano H, Blendy JA, Montell C. Musashi, a neural RNA-binding protein required for Drosophila adult external sensory organ development. Neuron 1994;13:67–81.

O'Guin WM, Sun TT, Manabe M. Interaction of trichohyalin with intermediate filaments: three immunologically defined stages of trichohyalin maturation. J Invest Dermatol 1992;98:24–32.

Okano H, Kawahara H, Toriya M, Nakao K, Shibata S, Imai T. Function of RNA-binding protein Musashi-1 in stem cells. Exp Cell Res 2005;306:349–56.

Oro AE, Higgins KM, Hu Z, Bonifas JM, Epstein EH, Jr, Scott MP. Basal cell carcinomas in mice overexpressing sonic hedgehog. Science 1997;276:817–21.

Paladini RD, Saleh J, Qian C, Xu GX, Rubin LL. Modulation of hair growth with small molecule agonists of the hedgehog signaling pathway. J Invest Dermatol 2005;125:638–46.

Park SM, Deering RP, Lu Y, Tivnan P, Lianoglou S, Al-Shahrour F, et al. Musashi-2 controls cell fate, lineage bias, and TGF-beta signaling in HSCs. J Exp Med 2014;211:71–87.

Plikus MV, Baker RE, Chen CC, Fare C, de la Cruz D, Andl T, et al. Self-organizing and stochastic behaviors during the regeneration of hair stem cells. Science 2011;332:586–9.

Plikus MV, Guerrero-Juarez CF, Ito M, Li YR, Dedhia PH, Zheng Y, et al. Regeneration of fat cells from myofibroblasts during wound healing [e-pub ahead of print]. Science; http://dx.doi.org/10.1126/science.aai8792 (accessed 5 January 2017).

Plikus MV, Mayer JA, de la Cruz D, Baker RE, Maini PK, Maxson R, et al. Cyclic dermal BMP signalling regulates stem cell activation during hair regeneration. Nature 2008;451:340–4.

Rentas S, Holzapfel NT, Belew MS, Pratt GA, Voisin V, Wilhelm BT, et al. Musashi-2 attenuates AHR signalling to expand human haematopoietic stem cells. Nature 2016;532:508–11.

Rompolas P, Greco V. Stem cell dynamics in the hair follicle niche. Semin Cell Dev Biol 2014;25–26:34–42.

Sakakibara S, Imai T, Hamaguchi K, Okabe M, Aruga J, Nakajima K, et al. Mouse-Musashi-1, a neural RNA-binding protein highly enriched in the mammalian CNS stem cell. Dev Biol 1996;176:230–42.

Sakakibara S, Nakamura Y, Satoh H, Okano H. Rna-binding protein Musashi2: developmentally regulated expression in neural precursor cells and subpopulations of neurons in mammalian CNS. J Neurosci 2001;21:8091–107.

Stenn KS, Paus R. Controls of hair follicle cycling. Physiol Rev 2001;81:449–94.

Sugiyama-Nakagiri Y, Akiyama M, Shibata S, Okano H, Shimizu H. Expression of RNA-binding protein Musashi in hair follicle development and hair cycle progression. Am J Pathol 2006;168:80–92.

Vidal VP, Chaboissier MC, Lutzkendorf S, Cotsarelis G, Mill P, Hui CC, et al. Sox9 is essential for outer root sheath differentiation and the formation of the hair stem cell compartment. Curr Biol 2005;15:1340–51.

Wang S, Li N, Yousefi M, Nakauka-Ddamba A, Li F, Parada K, et al. Transformation of the intestinal epithelium by the MSI2 RNA-binding protein. Nat Commun 2015;6:6517.

Yuan S, Li F, Meng Q, Zhao Y, Chen L, Zhang H, et al. Post-transcriptional regulation of keratinocyte progenitor cell expansion, differentiation and hair follicle regression by miR-22. PLoS Genet 2015;11:e1005253.